Two distinct oscillatory auxin signals define the plasticity of lateral rooting in *Arabidopsis thaliana*

Chengzhi Ren[1,2], Jule Bodendorf[1,2], Jürgen Kleine-Vehn[1,2]*

[1]Institute of Biology II, Molecular Plant Physiology (MoPP), University of Freiburg; Freiburg, 79104, Germany.
[2]Center for Integrative Biological Signalling Studies (CIBSS), University of Freiburg; Freiburg, 79104, Germany.
*Corresponding author. Email: juergen.kleine-vehn@biologie.uni-freiburg.de

Abstract

The so-called root clock defines lateral root pre-branch sites (PBS) but how these sites contribute to the root system architecture remains incompletely understood (*1*, *2*, *3*, *4*). Here we reveal in the model plant *Arabidopsis thaliana* that two distinct oscillatory systems for the phytohormone auxin coordinate the spatial and temporal identity of PBS, jointly defining the lateral root density. We followed auxin signalling dynamics for days and thereby detected a systemic auxin signal oscillating in the mature primary root, which is distinct from the previously described root clock at the root tip. While the root clock spatially primes the PBS in the growing root tip, the systemic oscillatory auxin signal temporally controls the auxin-dependent identity of these PBS. Light perception in the shoot defines the strength of the systemic auxin signal and thereby controls the auxin-reliant ability of PBSs to develop into lateral roots. Moreover, PHYB and CRY1 mediate the light-dependent integration of other environmental signals, such as ambient temperature, into the control systemic auxin signalling and lateral root density. Our work reveals how two spatially distinct oscillatory auxin signals define the plasticity of plant root development in response to fluctuating conditions.

De novo organogenesis is a hallmark of the remarkable plasticity and adaptability in plants. In the context of root system architecture, lateral root (LR) formation is a critical process that enhances nutrient and water uptake, providing stability and resilience. The LR density is tightly controlled and the sites of presumptive LR development are predetermined along the primary root axis through a mechanism, which involves the so-called "root clock" (*1*, *2*, *3*). The root clock generates an oscillatory signal of the phytohormone auxin in the elongation zone of the main root, thereby marking the LR pre-branch sites (PBS) (*2*). While the root clock is established as a mechanism for generating PBS, there is controversy regarding whether these sites consistently mark the exact locations of LR development (*4*). We used prolonged imaging of the synthetic, auxin-responsive DR5 promoter fused to a luciferase reporter (*pDR5::Luc*) (*2*) to visualize the nuclear auxin output signalling and therewith PBS dynamics for days at

constant light (120 μmol·m^{-2}·s^{-1}) and temperature (21°C) conditions. Therewith, we revealed that indeed a substantial fraction of the PBS lost the auxin signal in time and did not give rise to LR development (Fig. S1). We, hence, addressed the currently elusive mechanism that decisively defines the transient or persistent nature of the auxin-reliant PBS and its contribution to control LR density.

Light quantitatively controls a systemic oscillatory auxin signal

To analyze the long-term dynamics of DR5 luciferase activity, we utilize kymograph representations, which are graphical depictions of spatial position (top to bottom) over time (left to right), essentially capturing the dynamic changes along a segmented root in a single image. This approach allowed us to detect a systemic DR5 oscillatory behaviour along the entire primary root, including the PBS, being distinct from the spatially defined auxin oscillation zone of the root tip (Fig. 1A and B, and Fig. S2A). In our constant growth condition, the frequency of this systemic DR5 oscillatory behaviour followed a normal distribution (Anderson-Darling normality test, P-value = 0.4501) with a period of around 24 hours (Fig. 1C, and Fig. S2B). We subsequently assessed if environmental factors, such as light intensity affect this systemic oscillatory auxin signal. When compared to control 120 μmol·m^{-2}·s^{-1} light conditions (hereafter referred to as high light, HL), a reduction of the light intensity to 50 μmol·m^{-2}·s^{-1} (hereafter referred to as medium light, ML) did not affect the frequency of the systemic auxin oscillations (Anderson-Darling normality test, P-value = 0.177) (Fig. 1, D and E, and Fig. S2, C and D) but did quantitatively decrease the overall intensity of the systemic auxin signal (Fig. 1F). Notably, the systemic nuclear auxin signalling was undetectable at a light intensity of 20 μmol·m^{-2}·s^{-1} (hereafter referred to as low light, LL) (Fig. 1G, and Fig. S3).

Based on these results, we propose that light quantitatively controls a systemic oscillatory auxin signal. Next, we addressed whether the systemic auxin signalling dynamics contribute to the transient nature of auxin-reliant PBS. Notably, despite the varying strength of systemic auxin signalling at different light intensities, we observed similar quantities of PBS under HL, ML, and LL conditions (Fig. 1H), indicating that the initial priming of PBS is largely independent of light intensity. However, we observed a correlation between the impediment of systemic auxin signalling and a steep increase in transient auxin signal in PBS at LL conditions (Fig. 1I). This result suggests that light intensity contributes to maintaining the auxin-reliant identity of PBS, correlating with a quantitative impact on systemic auxin oscillation.

Systemic auxin signal oscillations define PBS identity

To specifically address the light dependency of already formed PBS, we monitored PBS formation in 5-day-old *pDR5::Luc* seedlings under HL conditions for 48 hours and afterwards exposed them either to LL conditions or maintained them under HL as a control. After transferring seedlings from HL-to-LL conditions, the systemic auxin signalling completely ceased, observing the last oscillatory peak after 8 hours (Fig. 2A,

and Fig. S4A). Additionally, although the total quantity of PBS was similar under both light conditions (Fig. S5), the HL-to-LL transfer revealed that light intensity is critical to maintaining auxin signalling in PBS when compared to seedlings kept in HL (Fig. 2, C and D). These findings confirm that light intensity is crucial to maintaining the systemic oscillatory auxin signal and PBS identity.

Contrariwise, we also monitored PBS formation in 5-day-old *pDR5::Luc* seedlings under LL conditions for 48 hours and subsequently transferred the seedlings either to HL conditions or kept them at LL as a control. In this condition, systemic auxin dynamics recovered around 18 hours after transferring from LL-to-HL (Fig. 2B, and Fig. S4B). Moreover, HL recovered auxin signalling in PBS when compared to those kept in LL (Fig. 2, C and D). This finding again pinpoints the positive impact of light on systemic auxin signalling and its ability to reactivate auxin-reliant PBS.

Next, we tested if the light-dependent gating of auxin in PBS indeed contributes to the reshaping of the root system architecture. To ensure the light effects are independent of LR priming, we transferred 7-day-old seedlings between different light conditions and analyzed three days later the LR appearance in a defined section of the main root (grown between days 4 and 7; see marks in Figure 2e). We observed a strong decrease in LR density when transferring roots from HL-to-LL compared to those maintained at HL (Fig. 2, E and F). Conversely, LR density significantly increased when transferring from LL-to-HL as compared to those kept at LL (Fig. 2, E and F). This set of data confirms that light conditions control auxin-dependent PBS and thereby LR density. Accordingly, we propose that light quantitatively controls systemic oscillatory auxin signals, thereby temporally gating the identity of previously primed PBS and ultimately LR spacing.

Systemic auxin signal controls PBS identity at high ambient temperature

Based on our data we hypothesize that a local auxin oscillation zone (root clock) enables the regular priming of PBS during main root growth, whereas a systemic oscillatory auxin signal could integrate various environmental information into lateral root spacing. To further test this assumption, we introduced variation in ambient temperature. Temperature and light signalling both play a crucial role in shaping root system architecture and are in part molecularly interconnected (*5*). However, the current literature presents conflicting findings, indicating that increased ambient temperature can have both stimulative and inhibitory effects on lateral rooting within and across different species (*6 – 12*). To shed light on this seemingly complex role, we initially tested whether temperature also affects auxin signalling dynamics in the root, we transferred 5-day-old *pDR5::Luc* seedlings from a controlled temperature of 21°C to a high ambient temperature (HT) of 29°C at constant HL condition. By monitoring the root luminescence after the transfer, we observed an overall increase of auxin signalling in the focal oscillation (root clock) zone (Fig. 3, A and B), which also correlates with an increased number of PBS (Fig. 3C). However, the vast majority of auxin-reliant PBS appeared transiently, being reflected in time by a severe systemic disruption of auxin signalling (Fig. 3, D and E, and Fig. S6). Our results suggest that HT imposes initially

a positive effect on initiating PBS but subsequently a negative effect on the systemic auxin signal along the primary root. Contrary to this observation, the lateral root primordia (LRP) (Fig. S7) and overall LR density (Fig. 3, F and G) were not inhibited by HT but showed even slight enhancement when compared to the control.

To further address this paradox, we extended our imaging of the auxin output signalling to 8 days. Thereby, we observed a recovery of the systemic auxin signalling along the entire root around 70 hours after transferring seedlings to HT conditions (Fig. 3H, and Fig. S8). The systemic peak in auxin correlates with the reactivation of PBS, ultimately resulting in an increase in persistent PBS at HT (Fig. 3I). Notably, the number of recovered, persistent PBS under this condition is remarkably similar to the number in the control temperature condition. The reactivation of PBS strictly occurs simultaneously or after recovery of systemic auxin peak (Fig. 3H, Fig. S8), suggesting again that a systemic auxin signal enables the environmental control of already primed PBS.

Light perception gates high temperature-dependent control of auxin-reliant PBS identity

To confirm that the systemic auxin signal indeed integrates environment information into lateral rooting, we quantitatively lowered the HT-induced recovery of the systemic auxin signal, using medium light conditions. Accordingly, we grew *pDR5::Luc* seedlings at 21°C and ML and transferred 5-day-old seedlings to HT and ML conditions. Similar to seedlings at HL (Fig. 3), HT also increased the auxin signalling output at the focal oscillatory zone (Fig. 4, A and B), correlating with initially enhanced PBS priming at ML conditions when compared to the control (Fig. 4C). Similar to the HL condition, the formed PBS showed transient auxin signals, being reflected by a strong, systemic disruption of auxin signalling in the mature root.

The HT also induced a temporal decline (Fig. 4, D and E, and Fig. S9) and systemic recovery of auxin signalling in ML conditions, but, importantly, the recovery of the systemic signal was as anticipated quantitatively reduced (Fig. 4H) when compared to HL conditions. Notably, the systemic auxin recovery was also temporarily delayed, occurring around 100 hours after the transfer (Fig. 4, F and G, and Fig. S10). In agreement with our assumptions, ML-dependent reduction in systemic auxin signal also reduced the recovery of auxin-reliant PBS (Fig. 4I) when compared to HL conditions. This set of data confirms that light-dependent, systemic oscillatory auxin signalling defines the transient or persistent nature of PBS. Moreover, our data suggests that light quantity gates the negative impact of HT on PBS progression.

We next tested whether the proposed light-dependent gating of ambient temperature indeed defines root system architecture. In contrast to the limiting effect of HT on LR density under HL conditions (Fig. 3), HT induced a strong reduction in the density under ML conditions (Fig. 4, J and K), confirming that light quantity indeed contextualizes the integration of ambient temperature into root system architecture.

Next, we tested if this gating mechanism defines not only PBS identity but also blocks the LRP development. Whereas the LR density was decreased in these conditions, it did not increase the number of non-emerged lateral roots but showed a quantitively similar amount of LRP when compared to the control condition (Fig. S11). This finding suggests that light-gated HT response does not primarily block LRP progression but impacts on PBS identity. In agreement with its impediment in systemic auxin signalling, we observed that the HT-dependent inhibition of lateral rooting was further enhanced under LL conditions (Fig. S12). This set of data indicates that systemic oscillation of auxin integrates environmental signals, such as light and temperature, into the temporal control of PBS, contributing significantly to the root system architecture. We hence propose that the effect of high ambient temperature on lateral rooting is conditional, which can explain the seemingly conflicting literature on high temperature and its impact on lateral rooting (*6 – 12*).

Besides its impact on lateral rooting, high temperature also enhances main root growth in an auxin-dependent manner (*13 – 15*). It has been proposed that the priming of lateral roots may depend on the interplay of auxin and main root growth dynamics (*16 – 17*). Therefore, we next aimed to address whether HT-induced main root growth is linked to lateral rooting under our conditions. HT induced main root growth in HL, but this effect was abolished in ML conditions, which is conversely to its impact on lateral rooting (Fig. S13, A and B). These findings indicate that HT affects lateral rooting and main root growth via distinct mechanisms.

Next, we used light exposure of the root or shoot only to dissect where the light signal that modulates lateral rooting is perceived. We found that light exposure of the shoot is not only essential for lateral root development but also sufficient to gate the temperature-dependent lateral rooting (Fig. S14, A–F). Hence, we assume that light perception in the shoot contributes to the auxin-reliant lateral rooting mechanism. Subsequently, we investigated the genetic mechanism of light-gated HT-dependent repression of lateral rooting. Mutations in the *phytochrome B* (*phyB*) red and far-red light photoreceptor caused hypersensitivity to HT-induced repression of lateral rooting at ML conditions when quantitatively compared to the wild-type (Fig. S15, A–C). In addition to functioning as a light sensor, PHYB also acts as a thermosensor (*18*). However, the increased hypersensitivity to HT-induced repression of lateral rooting observed in the *phyB-9* mutant suggests that PHYB does not function as the thermosensor in this process (Fig. S15, A–C). Moreover, we detected a similar hypersensitivity to HT at ML condition in mutants of the blue light receptor *cryptochrome 1* (*CRY1*) (Fig. S15, A–C). Notably, triple mutants of *phyBcry1cry2* not only enhanced hypersensitivity to HT-induced repression of lateral rooting at ML conditions compared to single mutants of *phyB-9* and *cry1-304* (Fig. S15, A–C), but also caused sensitivity to HT at HL conditions when compared to the wild-type, which was not observed in the single mutant of *phyB-9* and *cry1-304* (Fig. 4, L–N). In contrast, the genetic interference with *phytochrome A* (*phyA*) or *phototropins* (*PHOTs*) had no major impact on the high-temperature-induced repression of lateral root development (Fig. S16, A–E). We accordingly conclude that *PHYB* and *CRY1* jointly mediate the

light-gated integration of ambient temperature into the root system architecture.

PHYB and *CRY1* both mediate light signals by regulating *PHYTOCHROME INTERACTING FACTORS* (*PIFs*) and *ELONGATED HYPOCOTYL5* (*HY5*) module, which is also known to integrate light quality during the shade avoidance response into the rate of lateral rooting (*19 – 21*). However, neither the quadruple mutant *pif1,3,4,5* (*pifQ*), nor *hy5-215* mutant was distinguishable from the wild type in regards to HT-dependent lateral rooting under ML condition (Fig. S16, A and F–I). This suggests a molecularly distinct mechanism for the integration of light quality during shade avoidance and the light quantity-dependent gating of HT into lateral rooting.

Mechanistically, we reveal that the perception of light quantity in the shoot defines the strength of a systemic oscillatory auxin signal in the main root, thereby defining the auxin-dependent identity of lateral root PBS. The light-dependent, systemic auxin dynamics also gate HT-dependent control of PBS progression to lateral roots, suggesting a general mechanism for environmental signal integration. Conceptually, our work illustrates that two oscillatory systems define LR spacing. While a local auxin oscillation zone (root clock) regulates the regular priming of PBS during main root growth, the systemic oscillatory auxin signal along the main root integrates environmental information, such as light and temperature, to control the PBS identity in time and eventually its progression to become lateral roots. This framework reveals how plants mechanistically use two oscillatory signals of the same regulator to combine robustness and plasticity into *de novo* organogenesis.

References and Notes

1. De Smet I., et al., Auxin-dependent regulation of lateral root positioning in the basal meristem of Arabidopsis. *Development* **134**, 681–690 (2007).
2. Moreno-Risueno AM., et al., Oscillating Gene Expression Determines Competence for Periodic Arabidopsis Root Branching. *Science* **329**, 1306–1311 (2010).
3. Xuan W., De Gernier H., Beeckman T., The dynamic nature and regulation of the root clock. *Development* **147**, dev181446 (2020).
4. Kircher S., Schopfer P., The plant hormone auxin beats the time for oscillating light-regulated lateral root induction. *Development* **145**, dev169839 (2018).
5. Qi L., et al., Integration of light and temperature signaling pathways in plants. *J. Integr. Plant Biol.* **64**, 393–411 (2022).
6. González-García M. P., et al., Temperature changes in the root ecosystem affect plant functionality. *Plant Commun.* **4**, 100514 (2023).
7. Wang R., et al., HSP90 regulates temperature-dependent seedling growth in Arabidopsis by stabilizing the auxin co-receptor F-box protein TIR1. *Nat. Commun.* **7**, 10269 (2016).
8. Borniego M. B., Costigliolo-Rojas C., Casal J. J., Shoot thermosensors do not fulfil the same function in the root. *New Phytol.* **236**, 9–14 (2022).

9. Gray W. M., et al., High temperature promotes auxin-mediated hypocotyl elongation in Arabidopsis. *Proc. Natl. Acad. Sci. U. S. A.* **95**, 7197–7202 (1998).
10. Nagel K. A., Temperature responses of roots: impact on growth, root system architecture and implications for phenotyping. *Funct. Plant Biol.* **36**, 947–959 (2009).
11. Gladish D. K., Rost T. L., The effects of temperature on primary root growth dynamics and lateral root distribution in garden pea (Pisum sativum L., cv. "Alaska"). *Environ. Exp. Bot.* **33**, 243–258 (1993).
12. Vescio R., Abenavoli M. R., Sorgonà A., Single and Combined Abiotic Stress in Maize Root Morphology. *Plants (Basel)* **10**, 5 (2021).
13. Feraru E., et al., PILS6 is a temperature-sensitive regulator of nuclear auxin input and organ growth in Arabidopsis thaliana. *Proc. Natl. Acad. Sci. U. S. A.* **116**, 3893–3898 (2019).
14. Gaillochet C., et al., HY5 and phytochrome activity modulate shoot-to-root coordination during thermomorphogenesis in Arabidopsis. *Development* **147**, dev192625 (2020).
15. Ai H., et al., Auxin-dependent regulation of cell division rates governs root thermomorphogenesis. *EMBO J.* **42**, e111926 (2023).
16. van den Berg T., et al., A reflux-and-growth mechanism explains oscillatory patterning of lateral root branching sites. *Dev. Cell* **56**, 2176-2191 (2021).
17. Reyes-Hernández B. J., Maizel A., Tunable recurrent priming of lateral roots in Arabidopsis: More than just a clock? *Curr. Opin. Plant Biol.* **76**, 102479 (2023).
18. Jung J. H., et al., Phytochromes function as thermosensors in Arabidopsis. *Science* **354**, 886–889 (2016).
19. Pierik R., Ballaré C. L., Control of Plant Growth and Defense by Photoreceptors: From Mechanisms to Opportunities in Agriculture. *Mol. Plant* **14**, 61–76 (2021).
20. van Gelderen K., et al., Far-Red Light Detection in the Shoot Regulates Lateral Root Development through the HY5 Transcription Factor. *Plant Cell* **30**, 101–116 (2018).
21. Zeng J., et al., Arabidopsis cryptochrome-1 restrains lateral roots growth by inhibiting auxin transport. *J. Plant Physiol.* **167**, 670–673 (2010).
22. Reed J. W., et al., Phytochrome A and Phytochrome B Have Overlapping but Distinct Functions in Arabidopsis Development. *Plant Physiol.* **104**, 1139-1149 (1994).
23. Reed J. W., et al., Mutations in the gene for the red/far-red light receptor phytochrome B alter cell elongation and physiological responses throughout Arabidopsis development. *Plant Cell* **5**, 147-157 (1993).
24. Guo H., et al., Regulation of Flowering Time by Arabidopsis Photoreceptors. *Science* **279**, 1360-1363 (1998).
25. Leivar P., et al., Multiple phytochrome-interacting bHLH transcription factors repress premature seedling photomorphogenesis in darkness. *Curr. Biol.* **18**, 1815-1823 (2008).
26. Oyama T., Shimura Y., Okada K., The Arabidopsis HY5 gene encodes a bZIP protein that regulates stimulus-induced development of root and hypocotyl. *Genes Dev.* **11**, 2983-2995 (1997).
27. Mazzella M. A., Casal J. J., Interactive signalling by phytochromes and

cryptochromes generates de-etiolation homeostasis in Arabidopsis thaliana. *Plant Cell Environ.* **24**, 155-161 (2001).
28. Malamy J. E., Benfey P. N., Organization and cell differentiation in lateral roots of Arabidopsis thaliana. *Development* **124**, 33-44 (1997).

Acknowledgements

We thank Stefan Kircher and Andreas Hiltbrunner for providing seed materials and critically reviewing the manuscript; Stefan Kircher for assistance with root luminescence imaging and analysis; Deutsche Forschungsgemeinschaft (DFG) (DFG; 470007283 to J.K.-V. and CIBSS – EXC-2189; 390939984 to J.K.-V.) and Chinese Scholarship Council (CSC, 202006300036 to C.R.) for funding. **Author contributions:** C.R. and J.K.-V. designed the research; C.R. and J.B. performed the research; C.R. analyzed data; and C.R. and J.K.-V. wrote the paper. **Competing interests:** The authors declare no competing interests. **Data and materials availability:** Available on request.

Supplementary Materials

Materials and methods

Plant Materials

The *Arabidopsis thaliana* ecotype Columbia 0 (Col-0) and Landsberg (Ler) were used as the wild type in this study. The *pDR5:Luc* (*1*) is in the ecotype Col-0 accession and was received from Stefan Kircher. The mutants of *phyA-211* (*2*), *phyB-9* (*3*), *cry1-304* (*4*), *pif1,3,4,5* (*5*) and *hy5-215* (*6*) mutants are all in the Col-0 accession and were received from Andreas Hiltbrunner. The mutant of *phyBcry1cry2* (*7*) is in the ecotype Ler accession and was received from Stefan Kircher.

Growth conditions and treatments

The Arabidopsis seeds were sterilized for 2–5 minutes with 70% ethanol, followed by drying. After sterilization, the seeds were uniformly plated on one single line on square plates (12 × 12 × 1.5 cm). The plates contained 50 mL standard Murashige and Skoog solid medium, which is made of 0.8% agar, 0.5× Murashige and Skoog (MS) medium, and with 1% sucrose (MS+, no exogenous sucrose was added for MS-) (pH 5.9). Subsequently, the seeds were stratified for 2 days in 10 °C and dark conditions. Seeds were germinated on vertically positioned plates within a Weiss-Technik incubator (Fitotron SGC 2), exposed to top-providing illumination from LED white cultivation lights (16h day/8h night cycle) in 21 ºC and an irradiance of 120 μmol m^{-2} s^{-1}. Plates grow under the above control condition for 4 days (root quantification assay) or 5 days (luminescence monitoring assay) before subsequent experiments. For light conditions and HT treatment, two Weiss-Technik incubators were configured at either 21°C (control) or 29°C (HT), operating under constant light. Each incubator was outfitted with top LED white culture lights arranged across three distinct culture levels, featuring irradiances of 20, 50, and 120 (control) μmol m^{-2} s^{-1}.

Root quantification

For root phenotyping, surface-sterilized seeds were uniformly plated, stratified, and germinated on a square plate (12 × 12 × 1.5 cm) as described above. After germination under the control condition for 4 days, marking the position of the root tip, the 4-day-old seedlings were then transferred to the treatment condition (either 21°C or 29°C with light conditions set at 20, 50 or 120 μmol m^{-2} s^{-1}) for additional 3 days and the root tip positions were marked again. For lateral and primary root phenotyping, the plates were scanned at 600 dpi using an Epson V850Pro photonegative scanner at 24-hour intervals, starting from the 3rd day to the 10th day of treatments. The lateral roots between the two marked root section were counted manually from the images and the length of primary roots between two marked positions was measured automatically using the SNT plugin or manually with Fiji/ImageJ. The significance test was conducted in R using the t.test and aov functions.

Lateral root primordia quantification

To phenotype lateral root primordia, seeds were placed on individual square plates. After marking the root tips of 4-day-old seedlings, they were moved to specific treatment conditions as outlined in the manuscript and figure legend (either 21°C or 29°C with light conditions set at 50 or 120 μmol m^{-2} s^{-1}). Following a 3-day treatment, the positions of the root tips were marked again, and the plates were scanned to measure the length of the primary roots. After 5 days of treatment, primary roots located between two marked positions were harvested, followed by fixation and clearing in accordance with a previously published protocol (*8*). The roots were mounted in 50% glycerol and analyzed using a Zeiss AxioObserver Z1 microscope (Plan-Apochromat 40×/0.95 objective) with a AxioCam MRc camera. Primordia were counted manually, and the length of primary roots between two marked positions was determined as described above. The significance test was conducted in R using the aov functions.

Luminescence imaging and analysis

The luciferase activity in roots was visualized by time-lapse imaging of seedlings sprayed with 2 mM luciferin (Biosynth AG, Switzerland). *DR5::Luciferase* seedlings were grown using the general procedure as described above. To perform time-lapse imaging of the DR5:Luciferase expression in the oscillation zone, a Vers Array XP camera system (Roper Scientific) was used to image the luciferase signal in the vertical growing Arabidopsis root tip from 5 days old (4 to 8 seedlings) with the set-up of the exposure times of 5 min (binning 2) interrupted by 14 min LED WL (measured irradiances of 10~30 μmol m^{-2} s^{-1} for low light, 40~60 μmol m^{-2} s^{-1} for medium light and 110~130 μmol m^{-2} s^{-1} for high light condition) followed by 1 min darkness. The temperature in the imaging chamber was configured at either 21°C or 29°C by a recirculating Cooler (JULABO FL300). Image sequences were saved for further analysis in Fiji/ImageJ. Image sequences were converted into kymographs by tracking the final course of root growth. This visualization captures spatiotemporal changes in

Luciferase signals during primary root growth. To quantify the universal DR5 signal in primary roots, the grey value of the primary root excluding the tip to the oscillation zone was recorded from the kymograph at an interval of every 10 hours. The PBS were counted manually from the kymographs and original image sequences. The length of primary roots was measured manually from the original images. To determine the time and strength of the systemic DR5 signal in primary roots, the time point and grey value were recorded when the systemic DR5 signal in the primary roots reached the top value. All measurements were performed with Fiji/ImageJ. The significance test was conducted in R using the t.test and aov functions. The Anderson-Darling normality test was conducted in R using the ad.test function.

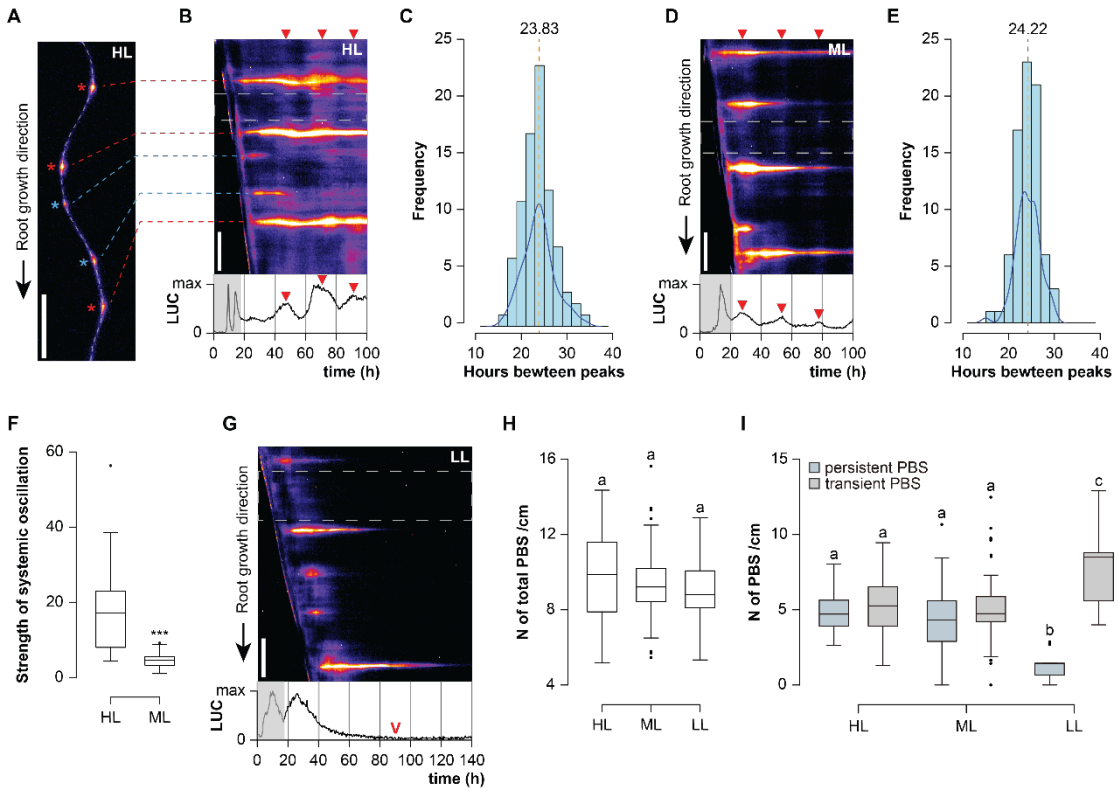

Fig. 1 Light quantitatively defines a systemic auxin oscillation in main roots and pre-branch sites.

(A-G) *pDR5::Luc* expressing root (**A**) was segmented (dashed line) for the respective kymograph (**B**). Asterisks and dashed lines mark the positions of persistent (red) and transient (blue) auxin signals in PBS. Kymographs display auxin signalling dynamics in high light (HL) (**B**), medium light (ML) (**D**) and low light (LL) (**G**) (Scale bar = 1 mm). Quantification of real-time luminescence is below the kymographs where the red triangles mark oscillatory peaks of systemic auxin signal (**B, D**). Red arrowhead denotes the downregulation of the systemic auxin signal (**G**). The dashed grey rectangle in the kymographs mark the region for the real-time plots. Quantified distribution of the time intervals between oscillatory peaks of systemic auxin under **(C)** HL and **(E)** ML conditions (mean value marked by a yellow dashed line; n = 23 to 29). **(F)** Quantified luminescence intensity of oscillatory peaks under HL and LL conditions (n

= 20). **(H)** Quantification of PBS density under HL, ML and LL conditions (n = 16 to 66). **(I)** Quantification of persistent and transient auxin in PBS under HL, ML and LL conditions (n = 16 to 66). Paired and two-tailed student's t-test performed for **(F)** ($p < 0.001$***). Letters indicate values with statistically significant differences from one-way ANOVA performed for **(H)** ($p > 0.05$) and **(I)** ($p < 0.0001$).

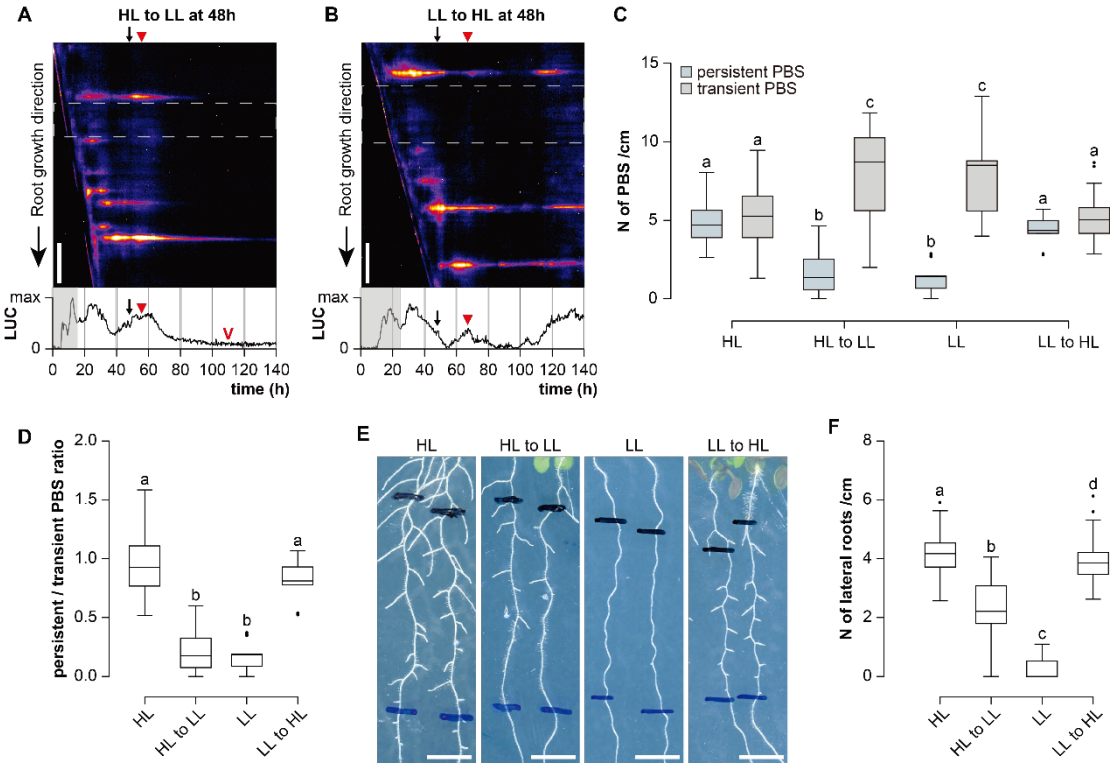

Fig. 2 Light-reliant systemic auxin signal determines PBS dynamics and lateral rooting.

(**A-D**) Kymograph and real-time quantification of relative luminescence show systemic auxin and PBS progression dynamics during light transitions from high light (HL) to low light (LL) **(A)** and LL-to-HL **(B)**. Black arrows mark the time of transfer; The red triangle marks the peak of the systemic auxin signal; The red arrowhead indicates that auxin signalling has reduced to the background level; The dashed grey rectangle marks the region for the real-time plots; The shaded area in real-time plots marked the signal originating from the root tip and root clock zone (Scale bar = 1 mm). Quantification **(C)** and the corresponding ratio **(D)** of persistent and transient auxin signal in PBS under both transitional and maintained light conditions (n = 16 to 38). **(E-F)** Representative images of root systems (**E**) and quantification of LR density **(F)** under both maintained light conditions and transferred HL-to-LL and LL-to-HL (n = 58 to 61; Scale bar = 5 mm). Letters indicate values with statistically significant differences from one-way ANOVA performed for **(C)**, **(D)** and **(F)** ($p < 0.0001$ for all).

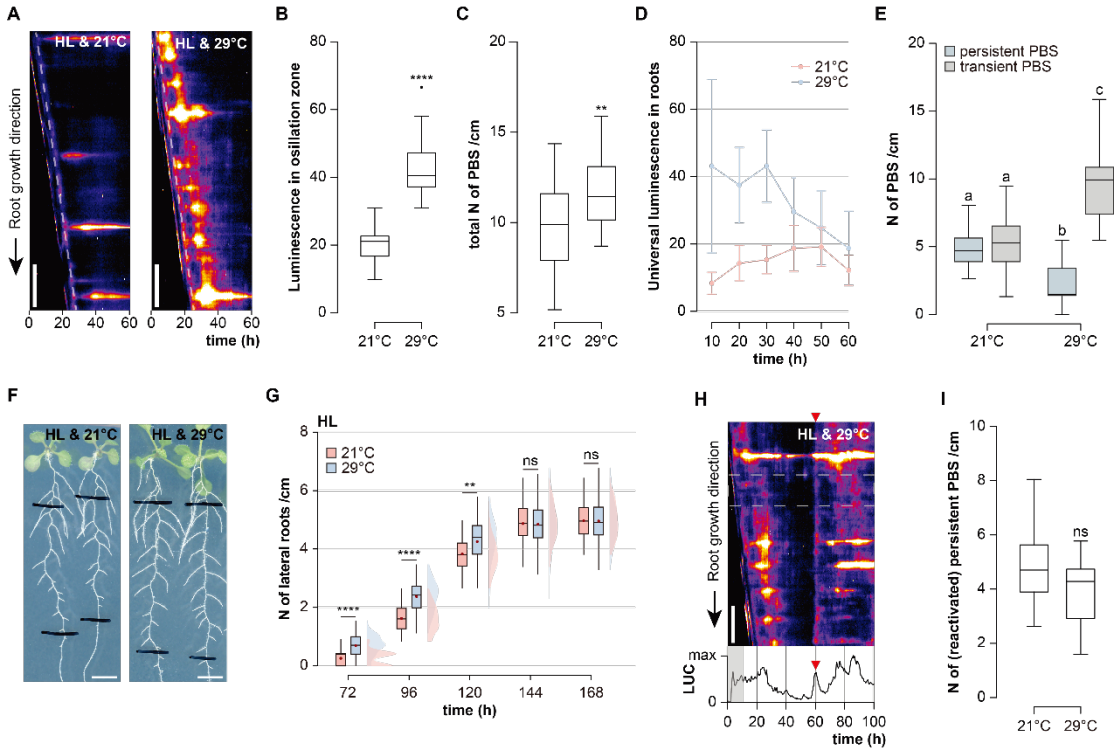

410

411 **Fig. 3 High-temperature affects systemic auxin signal and PBS dynamics.**

412 **(A)** Kymograph of *pDR5::Luc* expressing roots, showing the priming and progression
413 of PBS at 21°C and 29°C under high light (HL) conditions. The dashed line marks the
414 focal oscillatory (root clock) zone (Scale bar = 1 mm). **(B)** Quantification of average
415 luminescence in oscillatory zone over time in 21°C and 29°C under HL conditions (*n* =
416 24 to 30). **(C)** Quantification of PBS density at 21°C and 29°C under HL conditions (*n*
417 = 16 to 22). **(D)** The quantified dynamic of *pDR5::Luc* signal in the entire main roots
418 at 21°C and 29°C under HL conditions (Error bars represent standard deviation; *n* = 16
419 to 22). **(E)** Quantification of persistent and transient PBS at 21°C and 29°C under HL
420 conditions (*n* = 16 to 22). **(F-G)** Representative images of the root system (**F**) and time
421 series quantification of LR density **(G)** at 21°C and 29°C under HL conditions (*n* = 54
422 to 55; Scale bar = 5 mm). **(H)** Long-term kymographs and real-time quantification of
423 relative luminescence showing the recovery of systemic auxin and PBS under 29°C and
424 HL condition. The red triangle marked the recovery peak of systemic auxin signal; The
425 dashed grey rectangle marks the region for the real-time plots; The shaded area in real-
426 time plots marked the signal originating from the root tip and root clock zone (Scale
427 bar = 1 mm). **(I)** Quantified density of persistent PBS at 21°C and reactivated persistent
428 PBS at 29°C under HL condition (*n* = 16 to 22). Paired and two tailed student's t-test
429 performed for **(B**, **C**, **G** and **I)** ($p < 0.01$** and < 0.0001****). Letters indicate values
430 with statistically significant differences from one-way ANOVA performed for **(E)** ($p <$
431 0.0001).

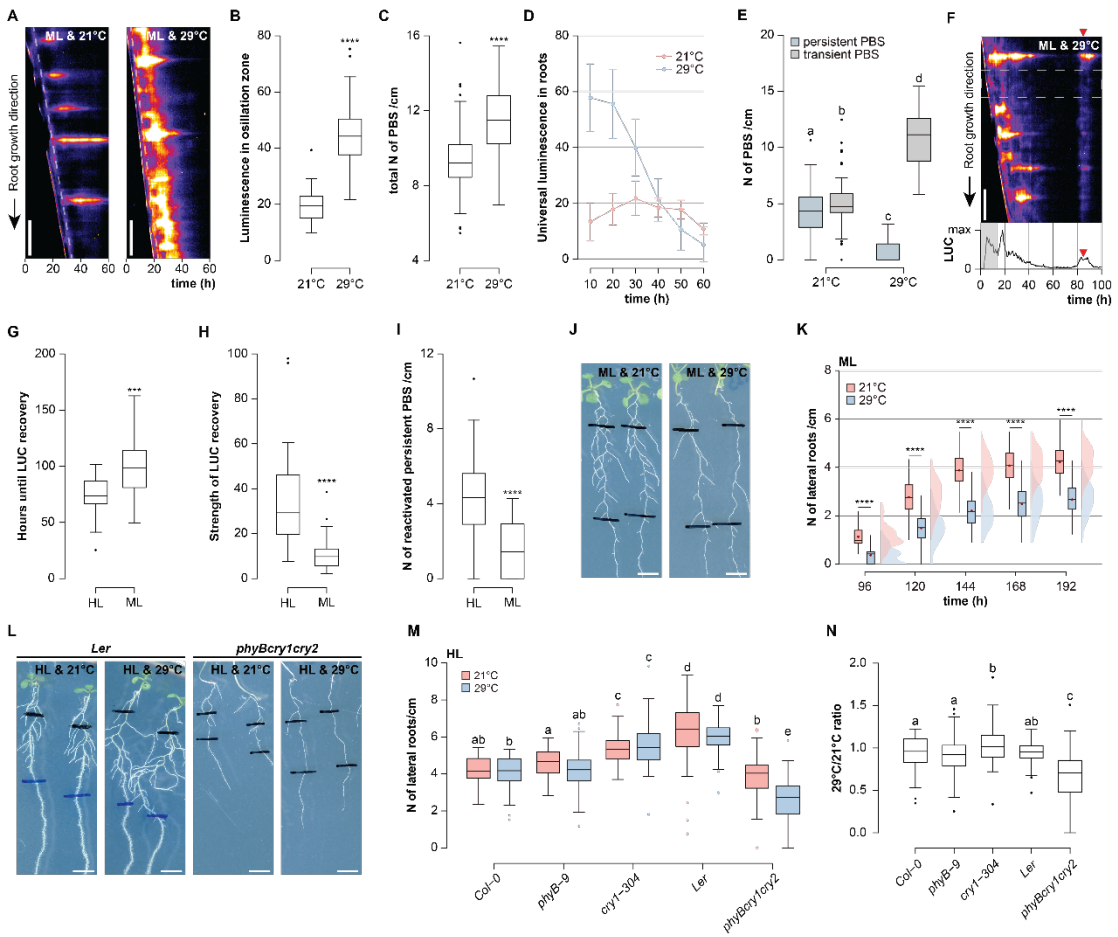

Fig. 4 Light gates high-temperature-dependent impact on systemic auxin signal and thereby lateral rooting.

(A) Kymograph of *pDR5::Luc* expressing roots, showing the priming and progression of PBS at 21°C and 29°C under medium light (ML) conditions. The dashed line marks the focal oscillatory (root clock) zone (Scale bar = 1 mm). **(B)** Quantifying average luminescence in oscillatory zone over time at 21°C and 29°C under ML conditions (n = 24 to 40). **(C)** Quantification of PBS density at 21°C and 29°C under ML conditions (n = 66). **(D)** Quantified dynamic of universal *pDR5::Luc* in main roots at 21°C and 29°C under ML conditions (Error bars represent standard deviation; n = 16 to 32). **(E)** Quantification of persistent and transient PBS at 21°C and 29°C under ML conditions (n = 66). **(F)** Long-term kymographs and real-time quantification of relative luminescence showing the recovery of systemic auxin and PBS at 29°C under ML condition. The red triangle marks the recovery peak of the systemic auxin signal; The dashed grey rectangle marks the region for the real-time plots; The shaded area in real-time plots marks the signal originating from the root tip and focal oscillation (root clock) zone (Scale bar = 1 mm). **(G-H)** Quantification of time until recovery **(G)** and strength **(H)** of systemic auxin signalling peak in primary roots after transferred at 29°C under ML and high light (HL) conditions (n = 24 to 48). **(I)** Quantified density of reactivated persistent PBS at 29°C under ML and HL conditions (n = 24 to 48). **(J-K)** Representative images of the root system **(J)** and time series quantification of LR

density **(K)** at 21°C and 29°C under ML conditions (*n* = 54 to 55; Scale bar = 5 mm). **(L-M)** Representative images (**L**) and quantified LR density **(M)** of *Col-0*, *Ler* wild types and light receptor mutants at 21°C and 29°C under HL conditions (*n* = 45 to 72; Scale bar = 5 mm). **(N)** Quantified ratio of LR density at 29°C to 21°C for *Col-0*, *Ler* wild types and light receptor mutants (*n* = 45 to 72). Paired and two-tailed student's t-test performed for **(B**, **C**, **G**, **H**, **I**, **K)** ($p < 0.001$*** and < 0.0001****). Letters indicate values with statistically significant differences from one-way ANOVA performed for **(E)**, **(M)** and **(N)** ($p < 0.0001$ for all).

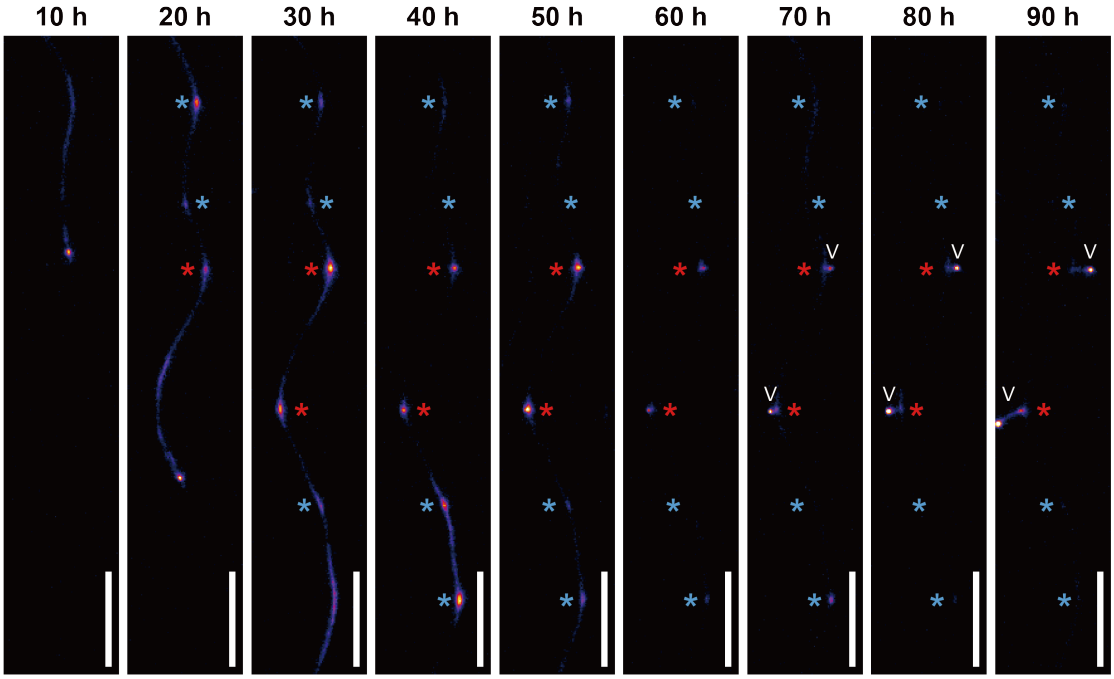

Fig. S1 Original images showing the distinct progression of persistent and transient PBS at HL condition.

Time series images of the primary root were taken every 10 hours under 21°C and high light (HL) conditions. Persistent PBS is marked by a red asterisk and transient PBS is marked by a blue asterisk. The white arrowhead denotes the emerged lateral root (Scale bar = 1 mm).

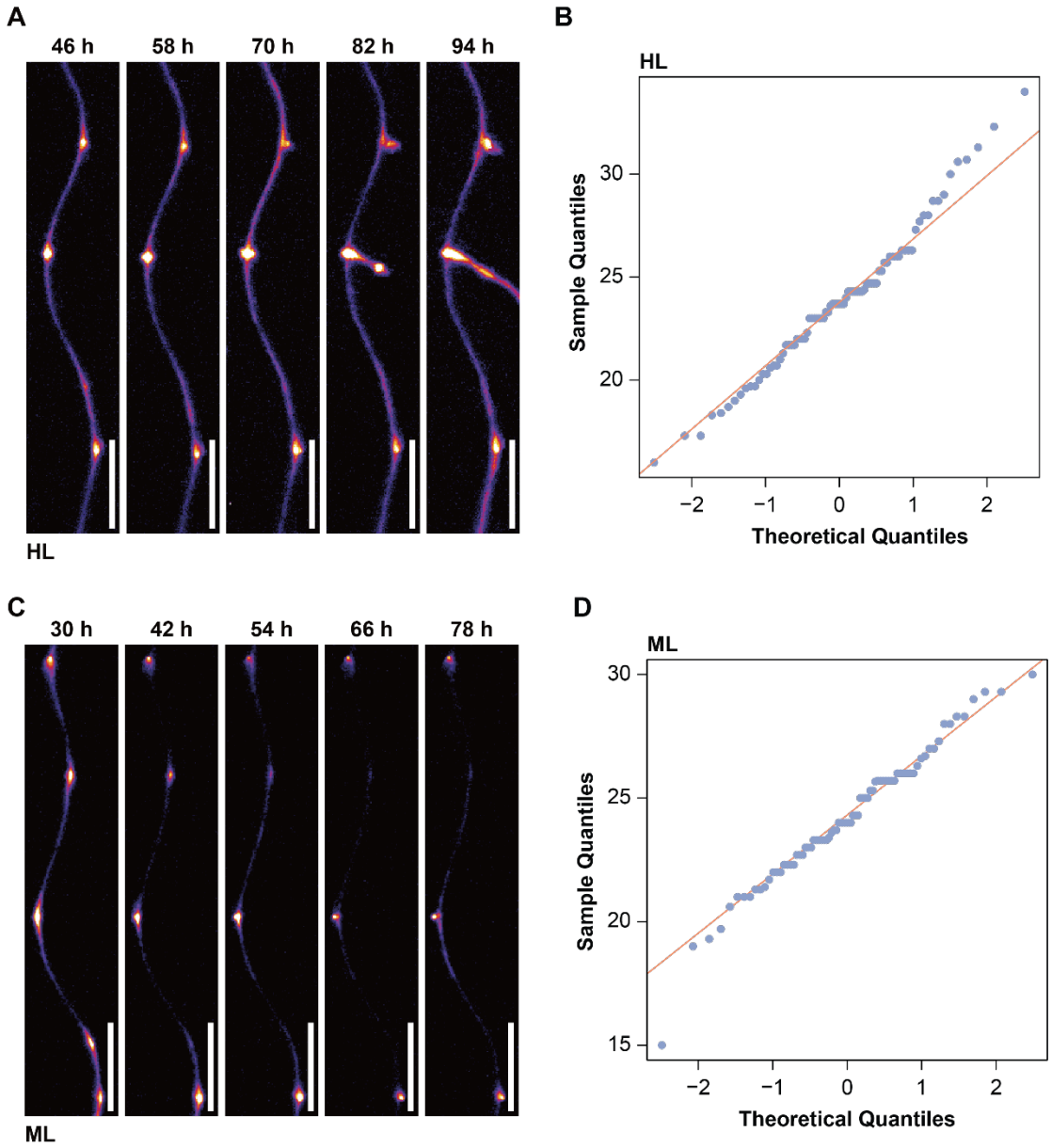

Fig. S2 The time intervals between oscillatory peaks of systemic auxin follow a normal distribution.

(**A and C**) Time series images of the primary root were taken every 12 hours under high light (HL) **(A)** and medium light (ML) **(C)** at 21°C conditions (Scale bar = 1 mm). (**B** and **D**) The quantile-quantile (Q-Q) plot compares the sample quantiles of the time intervals between peaks of systemic auxin oscillations with the corresponding theoretical quantiles of normal distribution at 21°C and light intensities of HL **(B)** and ML **(D)** conditions (n = 23 to 29). The pattern closely following the orange line indicates that the frequency of the systemic oscillation is likely to follow a normal distribution.

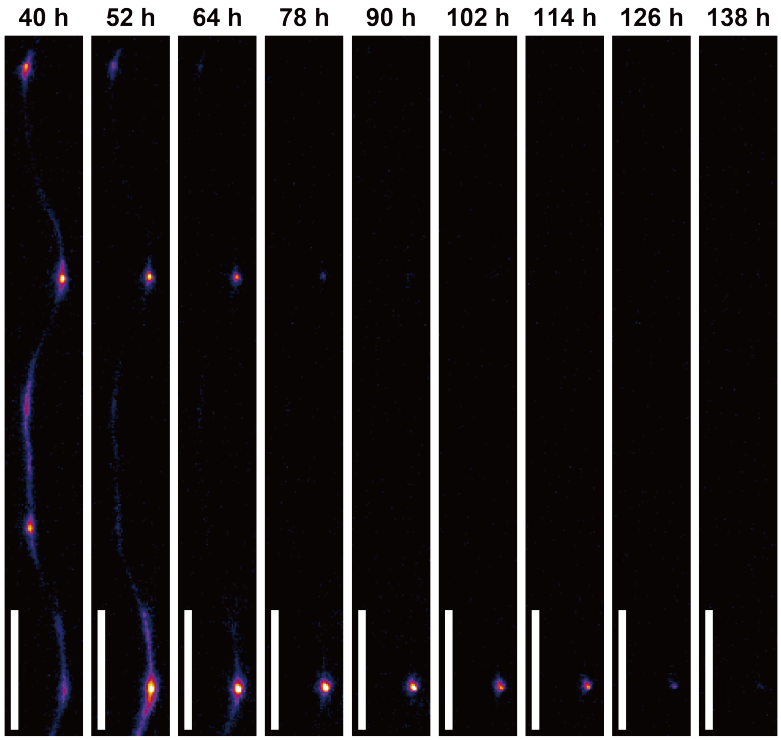

Fig. S3 Original images showing the dynamic of systemic auxin signal and progression of PBS at low light conditions.

Time series images of the primary root were taken every 12 hours under 21°C and low light (LL) conditions (Scale bar = 1 mm).

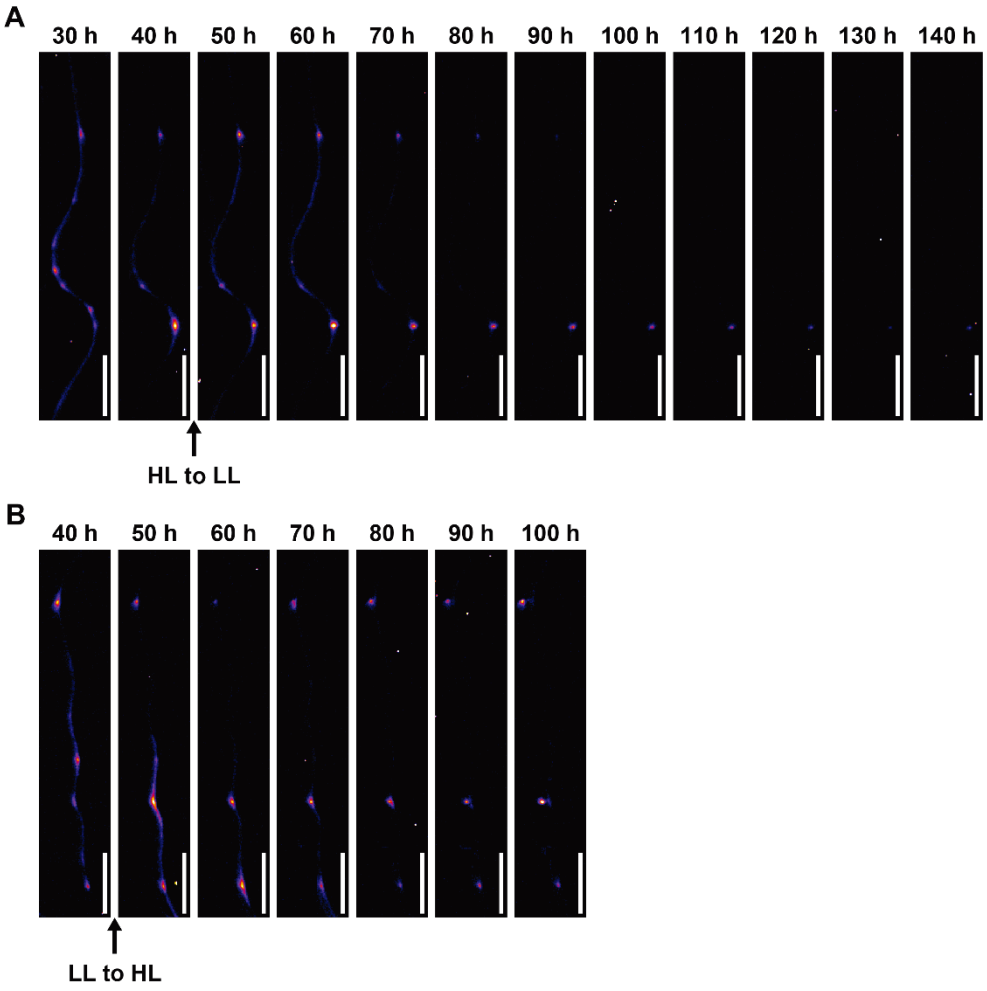

Fig. S4 Original images showing the dynamic of systemic auxin signal and progression of PBS during light transitions.

(**A-B**) Time series images of the primary root were taken every 12 hours under light transitional conditions from high light (HL) to low light (LL) **(A)**, and from LL-to-HL **(B)** (Scale bar = 1 mm).

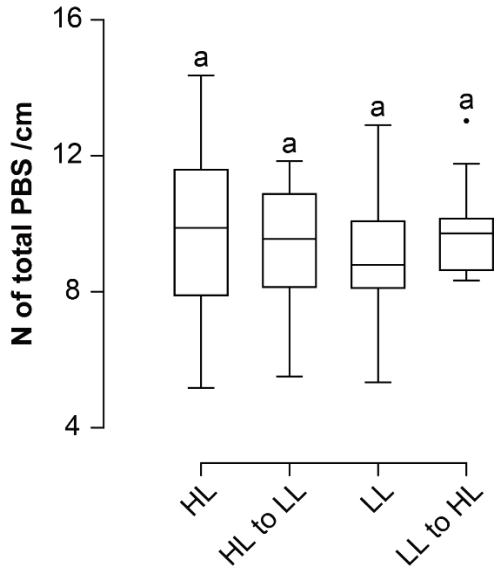

Fig. S5 The density of total PBS is quantitatively comparable at maintained and fluctuating light conditions.

Quantification of total PBS density under high light (HL), low light (LL) and transfer from HL-to-LL and LL-to-HL conditions (*n* = 16 to 38). Letters indicate values with statistically significant differences from one-way ANOVA performed ($p > 0.05$).

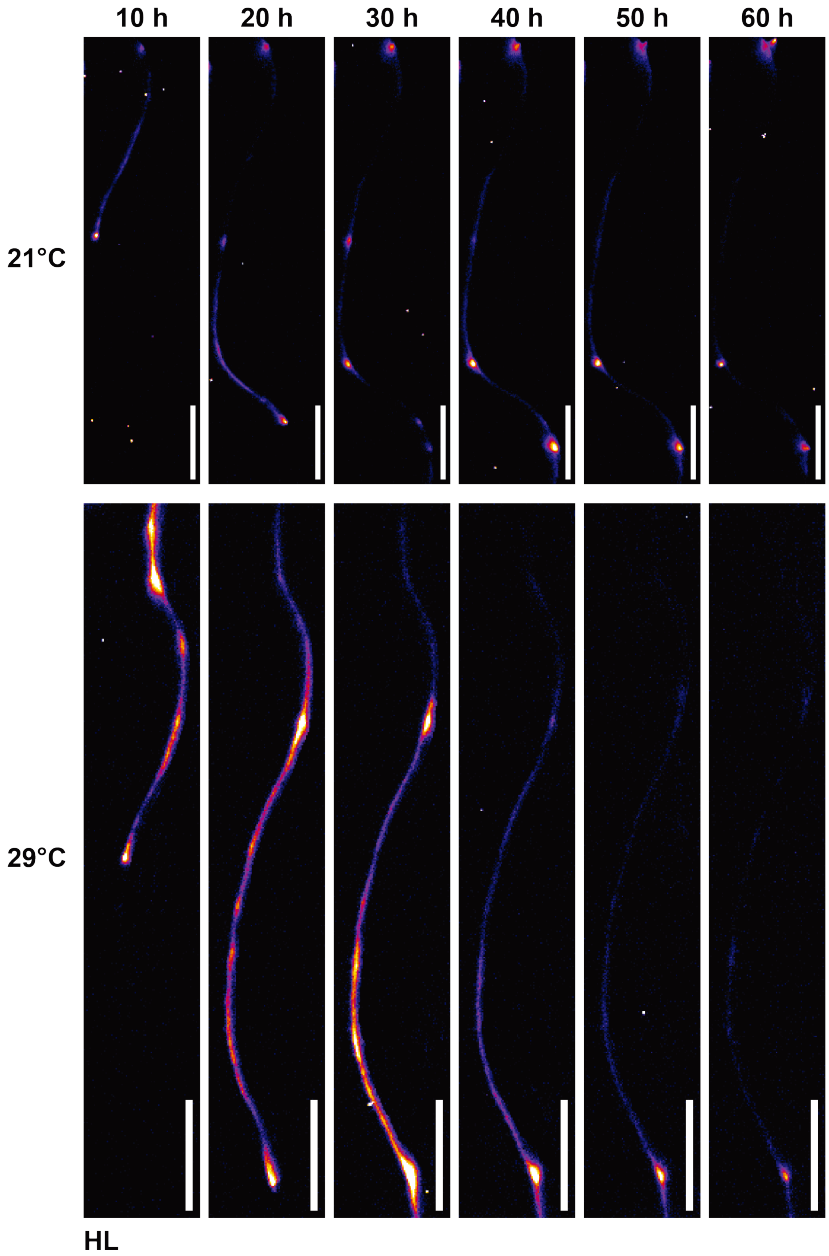

Fig. S6 Original images showing the dynamic of systemic auxin signal and progression of PBS under 21°C and 29°C at high light conditions.

Time series images of the primary root were captured every 10 hours under high light (HL) conditions at 21°C (top row) and 29°C (bottom row) (Scale bar = 1 mm).

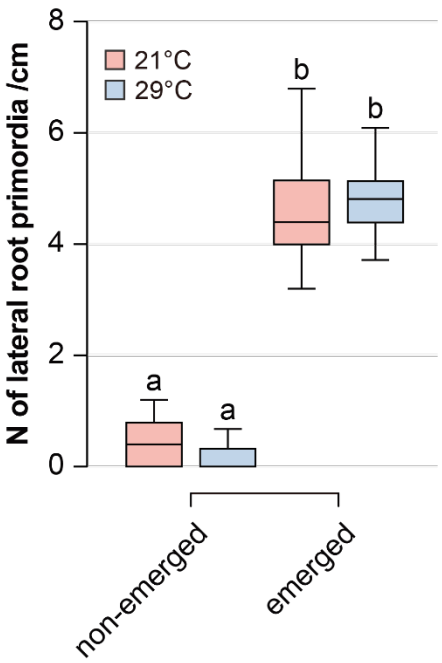

Fig. S7 Density of lateral root primordia is quantitively comparable between 21°C and 29°C at high light conditions.

Quantification of lateral root primordia density at 21°C and 29°C under high light (HL) conditions (*n* = 34 to 38). Letters indicate values with statistically significant differences from one-way ANOVA performed ($p < 0.0001$).

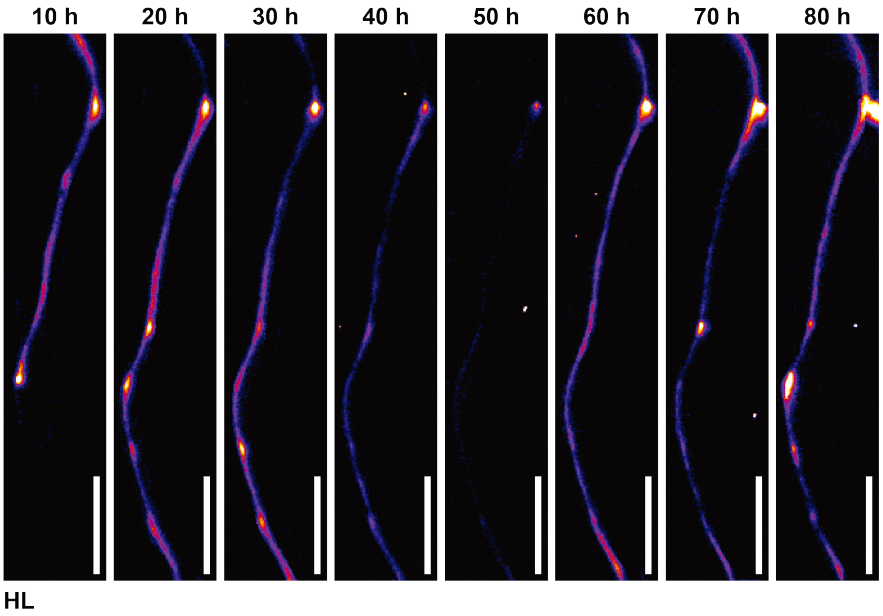

Fig. S8 Original images showing the recovery of systemic auxin signal and PBS under high temperature at high light conditions.

Time series images of the primary root were captured every 10 hours under high light (HL) conditions at 29°C. Scale bar = 1 mm.

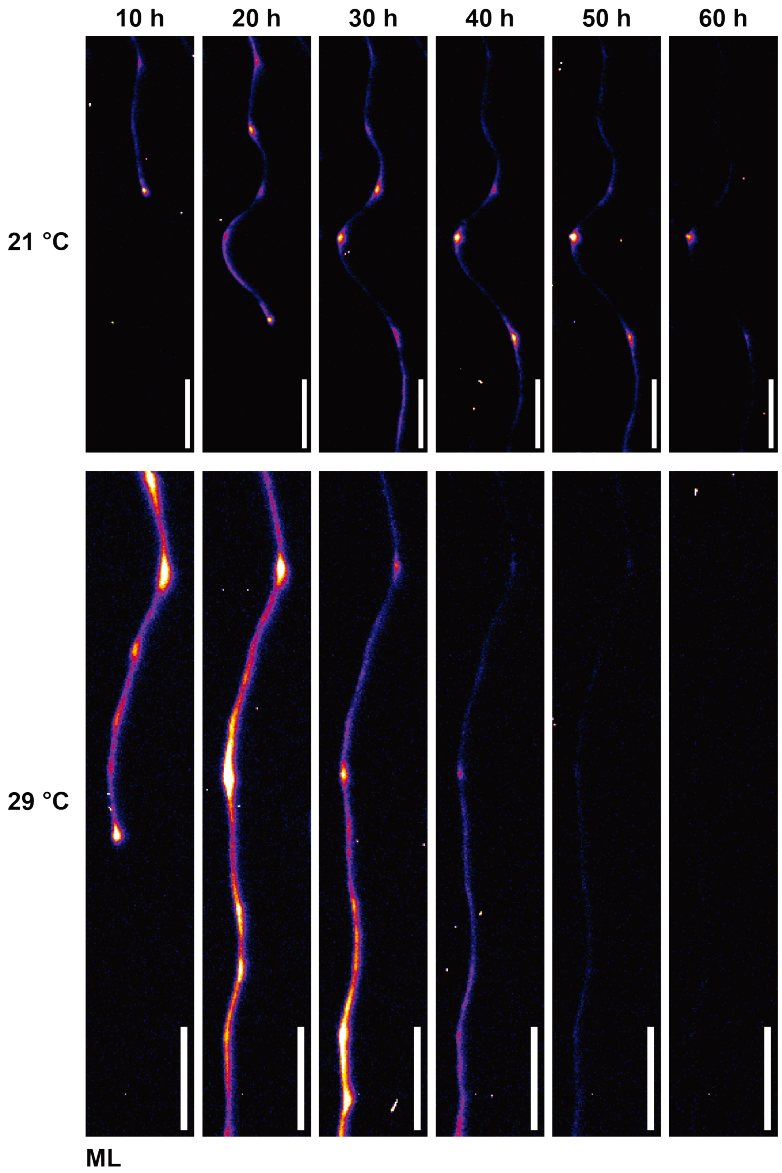

Fig. S9 Original images showing the dynamic of systemic auxin signal and progression of PBS under 21°C and 29°C at medium light conditions.

Time series images of the primary root were captured every 10 hours at 21°C (top row) and 29°C (bottom row) under medium light (ML) conditions (Scale bar = 1 mm).

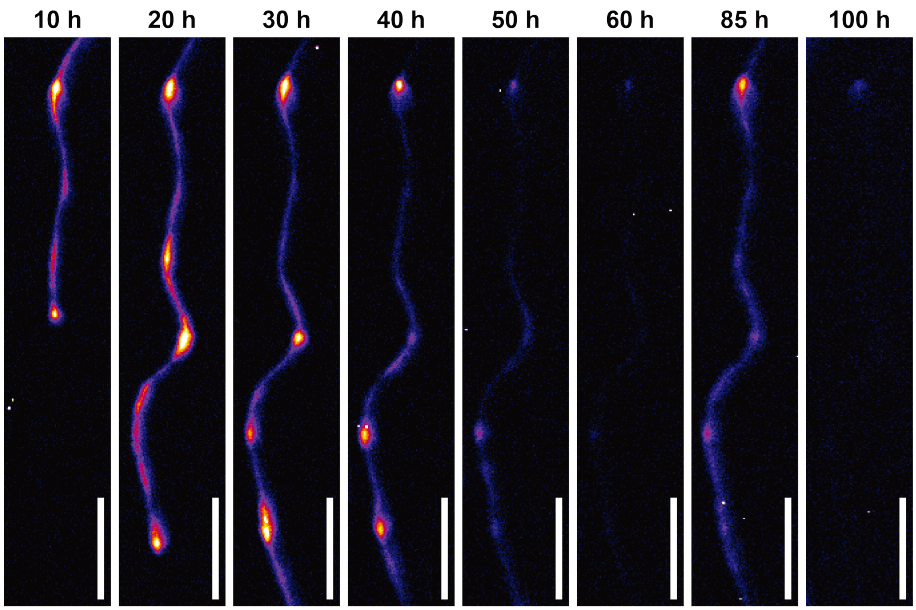

Fig. S10 Original images showing the recovery of systemic auxin signal and PBS under HT and ML conditions.

Time series images of the primary root were captured every 10 hours under 29°C and ML conditions (Scale bar = 1 mm).

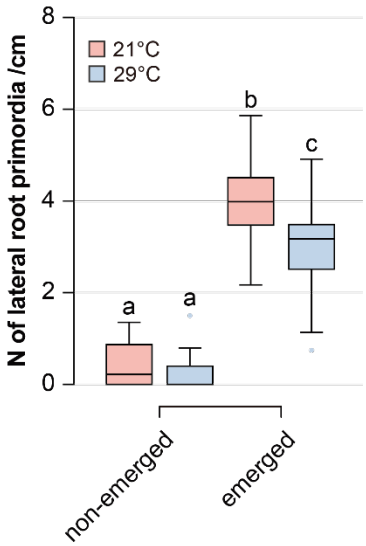

Fig. S11 Density of lateral root primordia under 21°C and 29°C at medium light (ML) conditions.

Quantification of lateral root primordia density at 21°C and 29°C under medium light (ML) conditions (n = 32 to 34). Letters indicate values with statistically significant differences from one-way ANOVA performed ($p < 0.0001$).

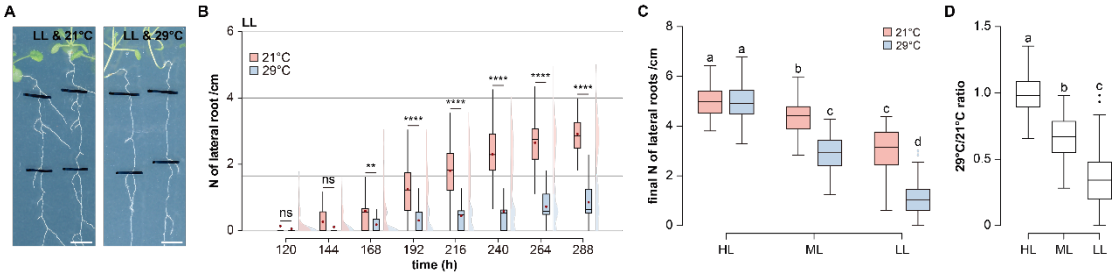

Fig. S12 Light quantity gates the high temperature-dependent inhibition of lateral root density.

(A-B) Representative images of root systems (**A**) and time series quantification of LR density **(B)** at 21°C and 29°C under low light (LL) conditions (*n* = 53 to 55; Scale bar = 5 mm). **(C-D)** Quantification (**C**) and calculated ratio **(D)** of final LR density at 21°C and 29°C under high light (HL), medium light (ML) and LL conditions (*n* = 53 to 55). Letters indicate values with statistically significant differences from one-way ANOVA performed for **(C)** and **(D)** ($p < 0.0001$ for both).

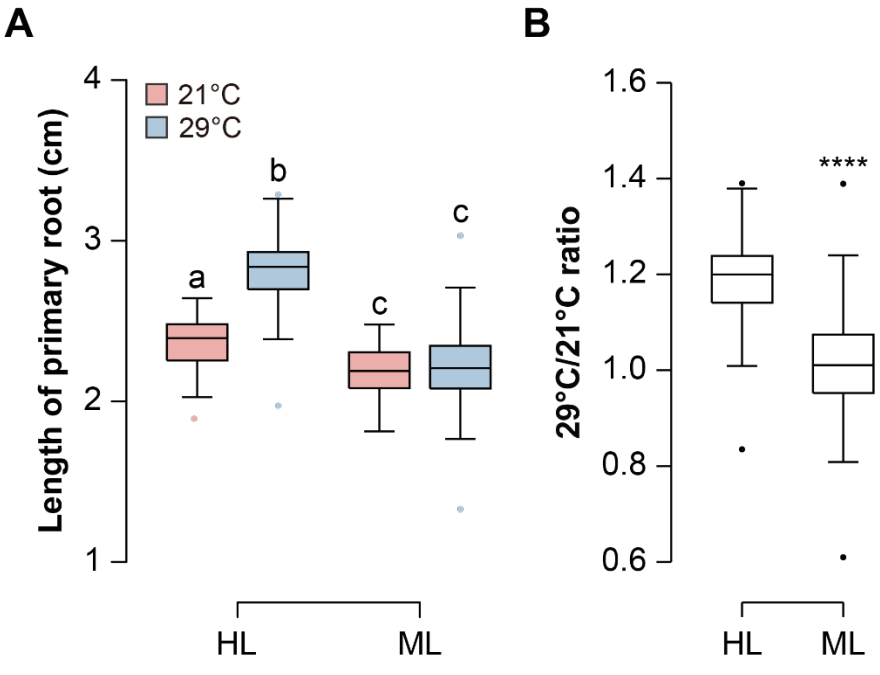

Fig. S13 HT-dependent elongation of the primary root relies on light.

(**A-B**) Quantification (**A**) and Calculated ratio (**B**) of primary root length of *Col-0* at 21°C and 29°C under high light (HL) and medium light (ML) (*n* = 54 to 55). Letters indicate values with statistically significant differences from one-way ANOVA performed for **(A)** ($p < 0.0001$). Paired and two-tailed student's t-test performed for **(B)** ($p < 0.0001$****).

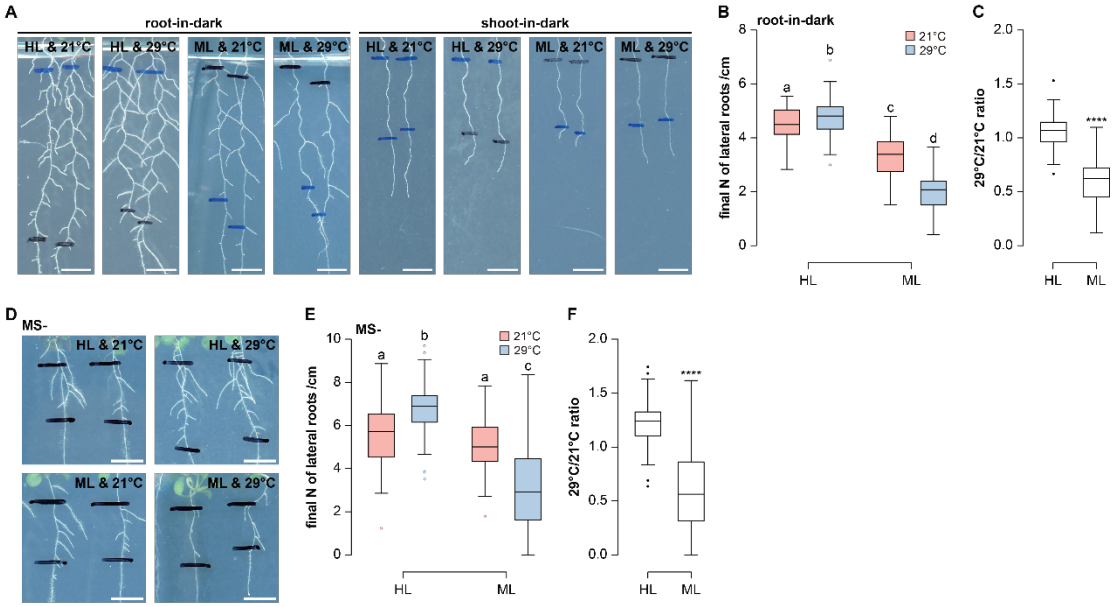

Fig. S14 Shoot-received light gates the high temperature-dependent inhibition of lateral root density.

(A) Representative images of root systems at 21°C and 29°C under root-in-dark and shoot-in-dark conditions(Scale bar = 5 mm). **(B-C)** Quantification **(B)** and calculated ratio **(C)** of LR density at 21°C and 29°C under root-in-dark conditions (n = 50 to 61). **(D)** Representative images of root systems at 21°C and 29°C under high light (HL) and medium light (ML) conditions on solid medium without sucrose (MS-) plates (Scale bar = 5 mm). **(E-F)** Quantification **(E)** and calculated ratio **(F)** of LR density of seedlings grown at 21°C and 29°C under HL and ML conditions on MS- plates (n = 47-51). Paired and two-tailed student's t-test performed for **(C)** and **(F)** ($p < 0.0001$**** for both). Letters indicate values with statistically significant differences from one-way ANOVA performed for **(B)** and **(E)** ($p < 0.0001$ for both).

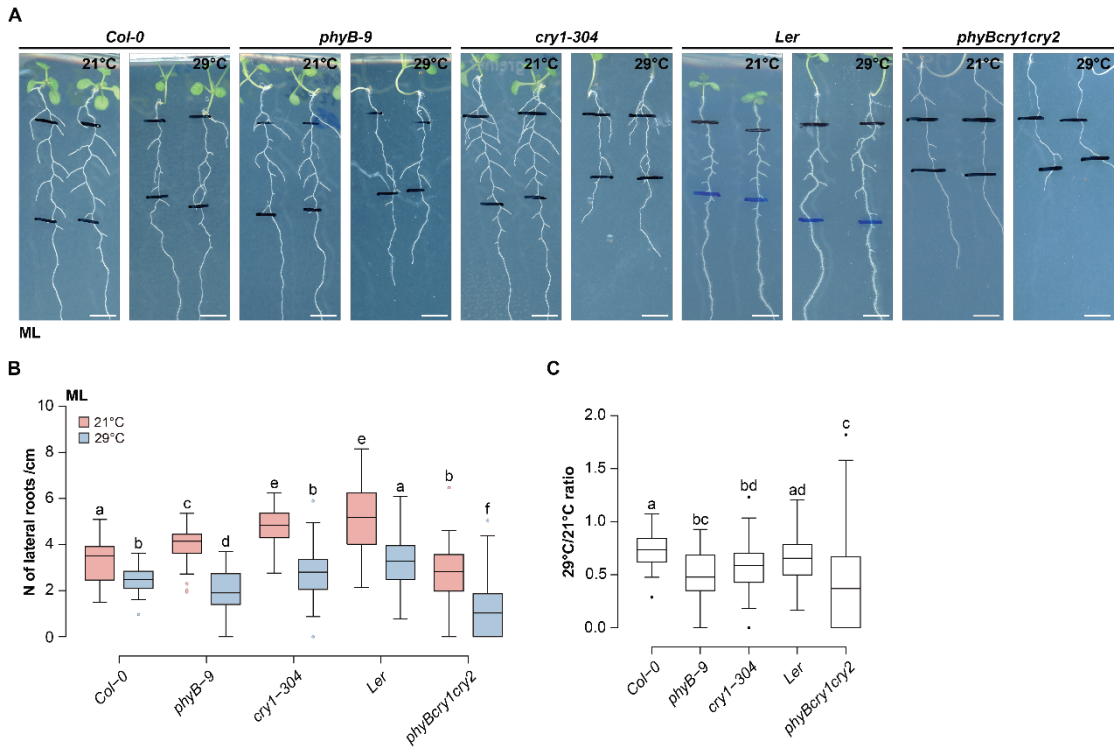

Fig. S15 The loss of PHYB and CRY1 enhances the HT-dependent inhibition of LR under ML conditions.

(A-C) Representative root system images (**A**) and quantification (**B**) as well as the calculated ratio (**C**) of LR density in *Col-0*, *phyB-9*, *cry1-304*, *Ler* and *phyBcry1cry2* at 21°C and 29°C under medium light (ML) conditions (n = 51 to 90; Scale bar = 5 mm). Letters indicate values with statistically significant differences from one-way ANOVA performed for **(B)** and **(C)** ($p < 0.0001$ for both).

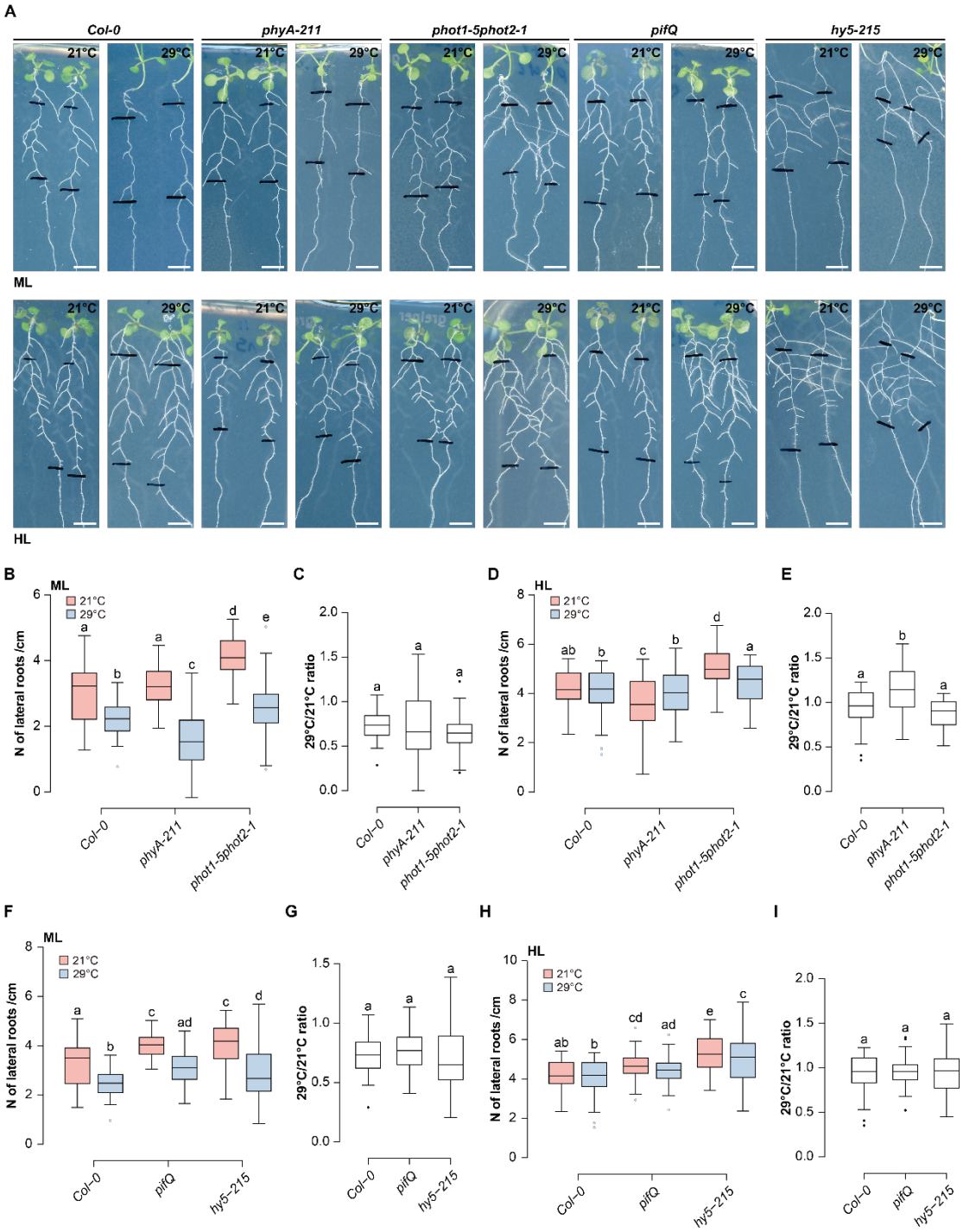

565

566 **Fig. S16 The inhibition of lateral rooting under high-temperature conditions in**
567 **light signalling mutants.**

568 **(A)** Representative root system images of wild-type *Col-0* and light signalling mutants
569 at 21°C and 29°C under medium light (ML) (top row) and high light (HL) (bottom row)
570 conditions (Scale bar = 5 mm). **(B)** Quantification and **(C)** calculated ratio of LR density
571 in *Col-0*, *phyA-211* and *phot1-5phot2-1* at 21°C and 29°C under ML conditions (n = 45
572 to 54). **(D-E)** Quantification **(D)** and calculated ratio **(E)** of LR density in *Col-0*, *phyA-*
573 *211* and *phot1-5phot2-1* at 21°C and 29°C under HL conditions (n = 52 to 54). **(F-G)**

Quantification **(F)** and calculated ratio **(G)** of LR density in *Col-0*, *pifQ* and *hy5-215* at 21°C and 29°C under ML conditions (n = 52 to 54). **(H-I)** Quantification **(H)** and calculated ratio **(I)** of LR density in *Col-0*, *pifQ* and *hy5-215* at 21°C and 29°C under HL conditions (n = 53 to 54). Letters indicate values with statistically significant differences from one-way ANOVA performed for **(B)**, **(D)**, **(E)**, **(F)** and **(H)** ($p < 0.0001$ for all) and for **(C)**, **(G)** and **(I)** ($p > 0.05$ for all).

Supporting References and Notes

1. Moreno-Risueno A. M., et al., Oscillating Gene Expression Determines Competence for Periodic Arabidopsis Root Branching. *Science* **329**, 1306–1311 (2010).
2. Reed J. W., et al., Phytochrome A and Phytochrome B Have Overlapping but Distinct Functions in Arabidopsis Development. *Plant Physiol.* **104**, 1139-1149 (1994).
3. Reed J. W., et al., Mutations in the gene for the red/far-red light receptor phytochrome B alter cell elongation and physiological responses throughout Arabidopsis development. *Plant Cell* **5**, 147-157 (1993).
4. Guo H., et al., Regulation of Flowering Time by Arabidopsis Photoreceptors. *Science* **279**, 1360-1363 (1998).
5. Leivar P., et al., Multiple phytochrome-interacting bHLH transcription factors repress premature seedling photomorphogenesis in darkness. *Curr. Biol.* **18**, 1815-1823 (2008).
6. Oyama T., Shimura Y., Okada K., The Arabidopsis HY5 gene encodes a bZIP protein that regulates stimulus-induced development of root and hypocotyl. *Genes Dev.* **11**, 2983-2995 (1997).
7. Mazzella M. A., Casal J. J., Interactive signalling by phytochromes and cryptochromes generates de-etiolation homeostasis in Arabidopsis thaliana. *Plant Cell Environ.* **24**, 155-161 (2001).
8. Malamy J. E., Benfey P. N., Organization and cell differentiation in lateral roots of Arabidopsis thaliana. *Development* **124**, 33-44 (1997).